

Detecting and distinguishing topological defects in future data from the CMBPol satellite

Pia Mukherjee,^{1,*} Jon Urrestilla,^{2,1,†} Martin Kunz,^{3,1,‡}
 Andrew R. Liddle,^{1,§} Neil Bevis,^{4,¶} and Mark Hindmarsh^{1,**}

¹*Department of Physics & Astronomy, University of Sussex, Brighton, BN1 9QH, United Kingdom*

²*Department of Theoretical Physics, University of the Basque Country UPV-EHU, 48040 Bilbao, Spain*

³*Département de Physique Théorique, Université de Genève, 1211 Genève 4, Switzerland*

⁴*Theoretical Physics, Blackett Laboratory, Imperial College, London, SW7 2BZ, United Kingdom*
 (Dated: May 26, 2022)

The proposed CMBPol mission will be able to detect the imprint of topological defects on the cosmic microwave background (CMB) provided the contribution is sufficiently strong. We quantify the detection threshold for cosmic strings and for textures, and analyse the satellite's ability to distinguish between these different types of defects. We also assess the level of danger of misidentification of a defect signature as from the wrong defect type or as an effect of primordial gravitational waves. A 0.002 fractional contribution of cosmic strings to the CMB temperature spectrum at multipole ten, and similarly a 0.001 fractional contribution of textures, can be detected and correctly identified at the 3σ level. We also confirm that a tensor contribution of $r = 0.0018$ can be detected at over 3σ , in agreement with the CMBpol mission concept study. These results are supported by a model selection analysis.

I. INTRODUCTION

Cosmological probes are reaching a sensitivity where they are able to meaningfully constrain models of the early Universe. Data compilations including Wilkinson Microwave Anisotropy Probe (WMAP) data [1–5] already indicate that the observed inhomogeneities are mostly due to primordial adiabatic scalar perturbations [6, 7]. However, there remains room for low-level contributions from other sources such as cosmic defects [8–11] and primordial tensor perturbations, believed to be generated by inflation alongside the scalars.

These will be detected primarily from the signal they produce in cosmic microwave background (CMB) polarization, in particular the B-modes which have yet to be detected and are a target for future probes. The possible detection of B-modes produced by primordial gravitational waves (tensor modes) is often referred to as the ‘smoking gun’ of inflation. The amplitude of the primordial gravitational wave background would provide strong constraints on high-energy physics models of inflation, including some appealing models coming from string theory/brane inflation. String/M-theory may thus be constrained by cosmological data: even though there exist models [12] that give rise to a measurable tensor-to-scalar ratio r , a fairly general prediction from string cosmology seems to be that the level of primordial gravitational waves, given by r , is very low ($r \ll 10^{-3}$, in some cases

even $r \sim 10^{-23}$). As emphasized by Kallosh et al. [13] it is hard to obtain an inflationary model coming from string theory which predicts measurably high primordial tensor modes. Thus, a future detection of r in the accessible range $r \gtrsim 10^{-2}$ – 10^{-3} would present important implications for string cosmology.

Another typical prediction of string cosmology is the production of cosmic (super)strings [14–16]. Indeed, cosmic strings are a quite general prediction from high-energy inflationary models within the Grand Unified Theory (GUT) framework [17]. Strings produced after inflation will also generate CMB anisotropies [18–20]. Cosmic strings are not the only possible cosmic defects in high-energy inflationary models: global monopoles, semilocal strings and textures are all examples of cosmic defects that could be created after inflation and remain consistent with the Universe we observe. Determining the nature of cosmic defects would provide invaluable information on high-energy symmetry breaking.

Defects produce scalar, vector and tensor perturbations. In contrast to the standard inflationary model, their vector perturbation modes do not die out since they are seeded continuously by the defects. Moreover, there are no free parameters that quantify the relative amount of scalar, vector and tensor perturbations independently, only an overall normalization factor; the relative amount of those perturbations is fixed for a given model. As defects produce vector and tensor modes, they create polarization B-modes directly [21–23]. It is interesting to note that even though cosmic defects can contribute at most a small fraction of the temperature perturbations, which must be mostly created by inflationary scalar modes to match the temperature anisotropy data, they can still be dominant in the B-mode spectra. Urrestilla et al. [24] have shown that Planck satellite [25] data would not suffer from significant degeneracy between tensors and strings. Thus, if Planck detects extra ingredients in the

*Electronic address: p.mukherjee@sussex.ac.uk

†Electronic address: jon.urrestilla@ehu.es

‡Electronic address: martin.kunz@unige.ch

§Electronic address: a.liddle@sussex.ac.uk

¶Electronic address: n.bevis@imperial.ac.uk

**Electronic address: m.b.hindmarsh@sussex.ac.uk

B-mode polarization spectra, its accuracy will be enough to say whether the source of the spectra are primordial tensor modes or cosmic defects.

CMBPol [26] is a proposed space mission that has higher sensitivity than Planck and is specifically designed to target the polarization anisotropies. Here we perform an analysis, partly along similar lines to Ref. [24], to determine both the detection threshold for different types of signal in CMBpol data and the ability of the satellite to distinguish between different defect types as well as primordial tensors. We use both parameter estimation and Bayesian model selection tools to achieve this. The detection thresholds we find improve on those expected from Planck over an order of magnitude, under realistic assumptions about foreground residuals and without assuming any level of delensing.

II. DIFFERENT COSMIC DEFECTS.

High-energy physics models of inflation often give rise to cosmic defects after inflation ends. The most studied ones are cosmic strings. These are one-dimensional objects that are extremely long (cosmic size) and yet microscopic in width, which generate CMB perturbations. They can arise in field theories (for example, they are expected in SUSY GUT models [17]) and can also be present as cosmic superstrings arising in fundamental string theories [14–16].

Other kinds of defects are also possible; global defects can be formed, such as global monopoles or textures [27–30]. Global monopoles do not present a problem in a cosmological setup (contrary to their local counterparts, the ‘usual’ magnetic monopoles), because their scaling properties are such that their energy density remains a fixed small fraction of the total. Textures are also permissible byproducts of cosmological symmetry breaking processes; indeed textures have been invoked in the CMB context as a possible explanation of the cold spot [31].

In previous papers by some of us [23, 29, 30, 32] we calculated the CMB power spectra (temperature and polarization spectra) of cosmic strings, semilocal strings [33, 34] and textures from field theoretical simulations. There we showed that the spectra from all these defects are very different from those of primordial inflationary models (including tensors). We also showed that even though there are similarities amongst them, there are also differences, with the semilocal predictions lying somewhere between textures and strings.

The zoo of possible defects is richer than that described here, but rather than performing an extensive comparison, we choose to focus on just two of them: cosmic strings and textures. An exhaustive analysis would not generate further insight at this stage. Besides, the exact prediction for each kind of defect has its subtleties, and often different calculational approaches result in slightly differing spectra [35]. Our aim is to verify and quantify at what level the spectra created by two different kinds

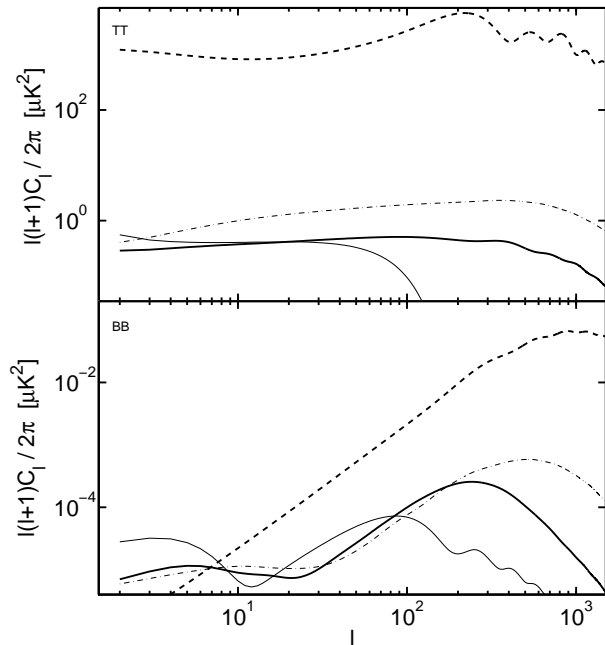


FIG. 1: The CMB temperature and B-mode polarization spectra for different components. The figure shows the temperature spectra from inflationary scalar modes (black dashed), inflationary tensor modes (black thin), cosmic strings (gray dot-dashed), and textures (black thick). The normalizations shown are at the threshold detection levels identified later in this paper assuming the true model is known: for the tensors this is at the $r = 0.0018$ level, for strings $f_{10}^{\text{st}} = 0.0012$, and textures $f_{10}^{\text{tex}} = 0.0005$. Clear differences are seen in the shapes of the spectra.

of defects, such as the ones shown in Fig. 1, can be distinguished by CMBpol.

We use the latest, more accurate, spectra derived from field theoretical simulations of cosmic strings and textures [36]. Those spectra have been obtained by making the minimal possible computational changes in order to capture the differences between those two defect types. The Abelian Higgs model used to model cosmic strings and the linear σ -model for the textures were evolved using the same discretization algorithms, the same type of initial conditions, and the same procedure to calculate the power spectra (more details can be found in Refs. [30, 32]). As in our previous papers, we quantify the amount of defects by f_{10} , which is the fractional contribution to the total TT power spectrum at $l = 10$. Observational data sets an upper limit on defects of a few percent: for strings $f_{10} \sim 0.1$ [10, 11] and for textures $f_{10} \sim 0.16$ [30]. In turn, this parameter f_{10} can be translated into a value of $G\mu$, with G the gravitational constant, and μ the string tension. For the Abelian Higgs model simulations used in this paper, $f_{10} = 0.1$ corresponds to $G\mu \simeq 6 \times 10^{-7}$.

For textures, it is not natural to talk about a “string” tension, but we will use μ defined as $2\pi\phi_0^2$, where ϕ_0 is the symmetry-breaking scale, to ease comparison (see the appendix of Ref. [30] for more details).

III. METHODS

We simulate CMBPol data as described in the CMBPol mission concept study [26] in its high-resolution version. The treatment there follows the approach of Ref. [37] in modelling residuals from foreground subtraction and propagating their effects into uncertainties in cosmological parameters.

We consider a flat Λ CDM model with the same set of fiducial parameters as used in Ref. [26]: $H_0 = 72 \text{ km s}^{-1} \text{ Mpc}^{-1}$, $\Omega_b h^2 = 0.0227$, $\Omega_c h^2 = 0.1099$, $\tau = 0.087$, $A_s = 2.41 \times 10^{-9}$, $n_s = 0.963$. In our analysis we vary these parameters in addition to the tensor-to-scalar ratio r and/or the level of strings and textures (for which we quote the level of these defects relative to the total TT power spectrum at multipole $l = 10$, which we label as $f_{10}^{\text{st, tex}}$). We assume the inflationary consistency relation $n_t = -r/8$ for the tensor spectral index, and do not allow running of the scalar spectral index. The inflationary parameters are specified at a pivot scale of $k_* = 0.05 \text{ Mpc}^{-1}$. We assume that 80% of the sky can be used for cosmological analysis.

The effect of lensing in the inflationary spectra is included in the prediction of the signal. We work in the Gaussian limit (ignoring mode correlations due to lensing or defects) where the likelihood takes its usual form [38], and ignore lensing due to defects. The task of detecting defects through B-modes primarily amounts to detecting the excess variance in the C_l from defects against this lensing contribution, which is more or less fixed by the other spectra. Accordingly its recovery is approximately limited by the cosmic variance of the lensing signal, but this is fully modeled through the likelihood. We use the pessimistic dust model (third column of Table 10 of Ref. [26]), and use an intermediate value for the level of foreground residuals (not 1% or 10%, but 5%).

We simulate instrumental data with the input sources being adiabatic primordial scalars plus either cosmic strings or textures at different contribution levels. We then analyze that data in two ways, the first being a parameter estimation exercise and the second a model comparison.

We use CosmoMC [39] to obtain parameter confidence contours. Our fiducial model consists of a flat Λ CDM model with the parameters quoted above, and we include some defects (one case with cosmic strings, the other with textures). Then we try to fit that simulated data using all the different possibilities that can be assembled from the different components: a model with strings; a model with tensors; a model with textures; a model with strings and textures; with strings and tensors; with textures and tensors; and with strings, tensors and textures. This

exercise allows us to infer the level of defects needed to clearly distinguish one from the other.

For our model-level analysis, we compute the Bayes factors of the set of models mentioned above, that is, models with one extra ingredient (strings, textures or tensors) and models with combinations of two of those or all three extra ingredients. In order to obtain the Bayes factors we use the Savage–Dickey ratio [40, 41], and we consider two sets of priors for these extra ingredients: flat linear priors and flat logarithmic priors. The relative Bayes factors of all these models will pinpoint which of those models is favoured and at which level.

We have also analysed the data under different assumptions than those described above. Ignoring foreground uncertainties reduces parameter error bars by about a factor of two. If we turn off lensing (i.e. assume that the CMB can be perfectly delensed) then error bars decrease by a factor of about seven. Thus, an order of magnitude improvement in f_{10} is still possible over the uncertainties described in the rest of this paper.

Previous works that considered constraints on strings in CMBPol-like experiments include Refs. [21] and [42]. However, the assumptions made there are different to those considered here regarding, for example, polarization sensitivities and lensing residuals. In addition, Ref. [21] uses the Unconnected Segment Model [43] for string perturbations, which has a different $G\mu$ for a given f_{10} unless special parameters are chosen [44].

IV. PARAMETER ESTIMATION ANALYSIS

We carry out two kinds of parameter estimation analyses. In the first, we fit assuming we already know the fiducial model used to generate the data. This enables us to determine the sensitivity of CMBpol to the different defect signals, under the best possible circumstances. We then carry out an analysis in the presence of model uncertainty, to assess the possible effect of mistaken assumptions.

A. Fitting with the correct model

If we assume we already know the correct model the analysis is particularly straightforward. We first use the fiducial model described above together with cosmic strings only, with $f_{10}^{\text{st}} = 0.0021$ (correspondingly, $G\mu \simeq 9 \times 10^{-8}$). Fitting for the same parameters as went into the model, strings are detected at high significance, with $f_{10}^{\text{st}} = 0.0021 \pm 0.0004$. Thus in this best-case scenario, a 0.0012 fractional contribution from cosmic strings ($G\mu \simeq 7 \times 10^{-8}$) would qualify for a 3σ detection, and hence this is the detection threshold for strings with this CMBpol configuration.

Repeating the analysis with textures, using a fiducial value of $f_{10}^{\text{tex}} = 0.0007$ ($G\mu \simeq 1.2 \times 10^{-7}$), we find that in fitting for textures $f_{10}^{\text{tex}} = 0.00070 \pm 0.00015$ is obtained.

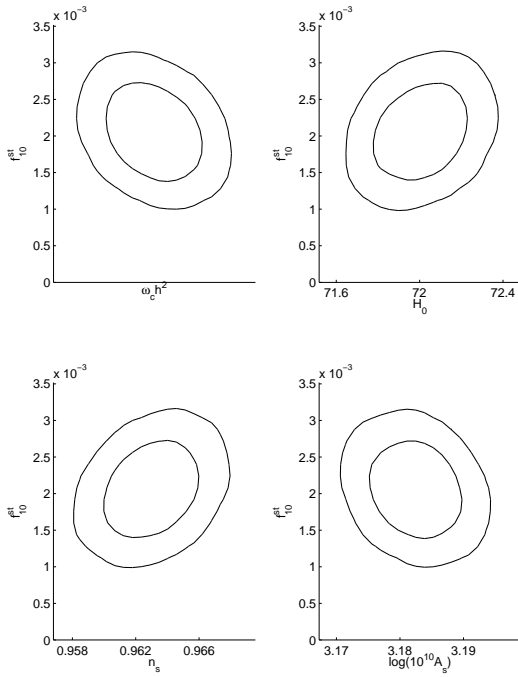


FIG. 2: The correlation between strings and cold dark matter density, the hubble parameter, the scalar spectral index, and the amplitude of primordial perturbations. These are the parameters with which strings are most correlated, at the -37%, 34%, 28% and -24% levels respectively. Textures are less correlated with cosmological parameters, the levels being -10%, 20%, 9%, and -8% respectively.

The 3σ detection threshold for textures is therefore a 0.0005 fractional contribution to the CMB TT power spectrum at $l = 10$ ($G\mu \simeq 1.0 \times 10^{-7}$).

The power spectra shown in Fig. 1 were normalized to indicate these detection thresholds. The distinct shapes of the spectra in both TT and BB are evident, with the defect spectra more resembling each other than the tensors.

B. Fitting with a range of models

In reality we do not know *a priori* which model is correct, and indeed our primary interest is likely to be in determining the correct model. One should be concerned about whether one might be able to draw conclusions based on the wrong model assumption, e.g. in the actual presence of strings, instead fitting primordial tensors and apparently detecting r at some significance. We wish also to know whether or not such data fits are able to draw us towards the correct model conclusion. The parameter estimation approach of this section is complemented by the more robust model-level analysis we provide in Section V.

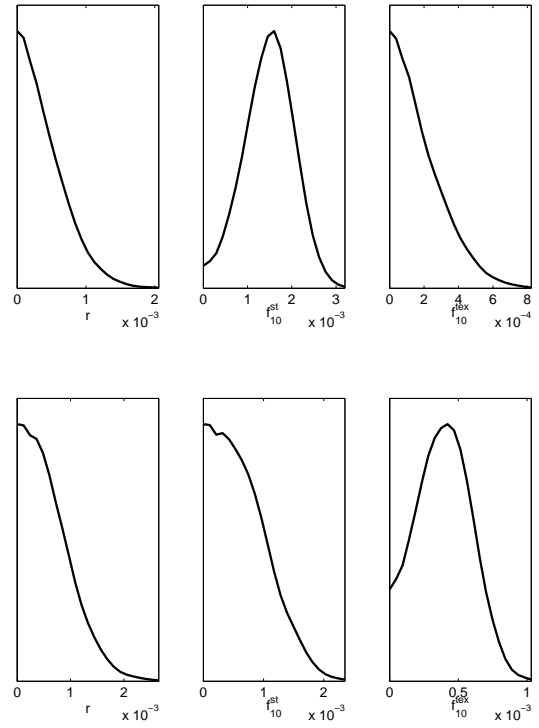


FIG. 3: 1D marginalized likelihood for tensors, strings, and textures, for the fiducial model with strings $f_{10}^{\text{st}} = 0.004$ (top row) and for the fiducial model with textures $f_{10}^{\text{tex}} = 0.0009$ (bottom row). In the texture case the peak is not strong enough for even a 2σ detection.

1. True model is strings

If we fit for tensors instead of strings, we do get a mild detection of r with $r = 0.0012 \pm 0.0005$, and other parameter recoveries are biased against their fiducial values; the ones that shift by more than a sigma are cold dark matter density (which goes up more than 1σ to 0.1103), the scalar spectral index (which goes down more than 1σ to 0.961) and H_0 (goes down more than 1σ to 71.8). Parameter correlations are shown in Fig. 2. If instead we wrongly fit for textures we get a strong detection of textures with $f_{10}^{\text{tex}} = 0.0006 \pm 0.00015$ and again other parameters get biased, though less significantly, as expected because textures can account for part of the string signal (cold dark matter density, scalar spectral index and H_0 shift to 0.1102, 0.962 and 71.8 respectively) There is therefore a danger of being led astray through assumption of the incorrect cosmological model. The bias in the values for other parameters is a potential signal but there may be no independent means of estimating them to the same accuracy. It is therefore important to test different model assumptions, and this motivates attempts to fit multiple components.

When fitting for strings and textures together, or for all of strings, textures and tensors, results are very similar. Figure 3 shows the marginalized likelihoods for each component from a fit where all parameters are simultane-

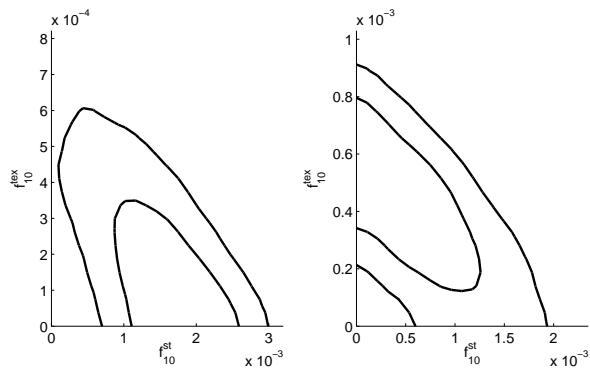


FIG. 4: The correlation between strings and textures in simulated CMBPol data with strings (left panel) and textures (right panel), showing 68% and 95% confidence contours.

ously varied, the upper panels showing a fiducial string model. From these likelihoods we get $f_{10}^{\text{st}} = 0.0015 \pm 0.0005$, while $f_{10}^{\text{tex}} < 0.0002$ (68% c.l.), 0.0005 (95% c.l.) and $r < 0.0005$ (68% c.l.), 0.0011 (95% c.l.) receive only upper limits. The level of correlation between strings and textures is found to be $\approx 60\%$, shown in Fig. 4. Tensors are not much correlated with strings (10%) or textures (15%) (Fig. 1 shows that strings peak at roughly twice as high an l as textures, and at low l strings have a little peak where the tensors dip, making strings a little more dissimilar to tensors than textures). Table I summarizes the uncertainties found under various assumptions.

The correct component can also be sought based on the quality of the fits, i.e. by looking at the best-fit and mean likelihoods achieved in the MCMC analysis. Strings+textures+tensors and strings alone lead to similar best-fit or mean log-likelihood, in each case being at least 3 better than with textures alone and 10 better than tensors alone. We conclude that at this fiducial string contribution, the model of tensors alone could be discounted, and strings favoured over textures, though not convincingly.

We find that a slightly higher fiducial value of $f_{10}^{\text{st}} = 0.003$ gives a 4σ detection ($f_{10}^{\text{st}} = 0.0024 \pm 0.0006$), in a joint fit, while the other components continue to receive upper limits. The recovered string fraction is underestimated because part of the string signal gets ascribed to textures in the fits. Such results would be a strong indication that strings were the right model, and a subsequent refit varying the string amplitude alone would remove this recovery bias. The 3σ threshold for identifying strings correctly in favour of these alternatives is therefore $f_{10}^{\text{st}} \simeq 0.002$ ($G\mu \simeq 9 \times 10^{-8}$).

2. True model is textures

If we fit for tensors instead of textures, we get a false detection $r = 0.0016 \pm 0.0005$, while other parameters do not get much biased away from their input values. Bi-

Model has	$\delta f_{10}^{\text{st}}$	$\delta f_{10}^{\text{tex}}$	δr
String	0.00041	—	—
String	—	0.00015	—
String	—	—	0.00052
String	0.00056	0.00026*	—
String	0.00055	0.00025*	0.00055*
Texture	—	0.00015	—
Texture	0.00041	—	—
Texture	—	—	0.00054
Texture	0.00071*	0.00019	—
Texture	0.00067*	0.00023*	0.00070*

TABLE I: Standard deviation achieved when trying to fit the data with a model with one, two or three extra components. In the string case the fiducial value is $f_{10}^{\text{st}} = 0.0021$, and for textures $f_{10}^{\text{tex}} = 0.0007$. In each block of five, the first section corresponds to fitting with the correct component, the second and third the wrong component, and the fourth and fifth fitting multiple components including the correct one. The stars (*) denote the cases when only upper limits are placed and the numbers quoted are the difference between the 68% and 95% upper limits. (Just in this table we quote accuracies to an additional significant figure as compared to the rest of the text.)

ases are smaller because textures are less correlated with cosmological parameters (see caption of Fig. 2). If we perform the fit for strings instead of textures, strings receive a false detection with $f_{10}^{\text{st}} = 0.0017 \pm 0.0004$, with very insignificant parameter shifts this time in the opposite direction. Thus in both cases a false detection of the wrong component occurs for the level of textures assumed in the fiducial model.

When all of textures, strings and tensors are fitted for, then the input level of textures proves to be too low for a clear detection. Instead all components receive upper limits: $f_{10}^{\text{tex}} < 0.0005$ (68% c.l.), 0.0007 (95% c.l.), $f_{10}^{\text{st}} < 0.0008$ (68% c.l.), 0.0015 (95% c.l.) and $r < 0.0008$ (68% c.l.), 0.0015 (95% c.l.); see the lower panels of Fig. 3. Thus a 0.0007 contribution of textures to the CMB TT power spectrum at $l = 10$ is not clearly detectable when fitting for these two additional parameters.

Study of best-fit and mean likelihoods will again enable a ranking of models considered, with models involving textures preferred by about 3 (6) as compared to models with just strings (tensors).

Further simulations show that $f_{10}^{\text{tex}} = 0.0010$ in the data gives a 3σ detection of textures ($f_{10}^{\text{tex}} = 0.0006 \pm 0.0002$) and $f_{10}^{\text{tex}} = 0.0012$ gives a 4σ detection of textures ($f_{10}^{\text{tex}} = 0.0009 \pm 0.0002$), in the case when all components are fitted. As above, a part of the texture signal gets ascribed to strings in the fits, reducing the recovered texture signal when strings are also allowed. The threshold for identifying textures correctly in favour of these alternatives thus is $f_{10}^{\text{tex}} \simeq 0.001$ ($G\mu \simeq 1.4 \times 10^{-7}$).

V. MODEL SELECTION ANALYSIS

Until we have uncovered the presence of defects, we are less interested in constraints on the defect parameters and more in the fundamental question whether there are any defects in the Universe, and if yes, which kind. This is a question of model selection rather than parameter estimation, and should be dealt with by computing Bayes factors between the different models, including a model with no extra ingredients.¹ In this section we will only consider the fiducial string model.

Before embarking on a model selection analysis, we need to consider the priors that we want to place on the parameters. Here we will look at two different priors. In the first one, we assume that the prior is uniform in f_{10} in the interval $[0, 1]$ for all extra contributions. This interval is much wider than the precision of CMBPol, which will lead to a significant “Occam’s razor” factor that the defect models need to overcome in order to be favoured against the no-defect baseline model. While this prior makes sense when looking for a signal that may be present at some level in the C_ℓ , it appears at least as natural to impose a prior which assumes that the phase transition in which the defects were generated happens with equal probability at an arbitrary energy scales with some cut-off. This leads to a prior that is uniform in $\log_{10} G\mu$ for cosmic strings, or more generally uniform in the logarithm of the amplitude. As limits we choose that the energy scales ($\sim \sqrt{\mu}$) would range from the GUT scale ($\sim 10^{16}$ GeV) to the SUSY breaking scale ($\sim 10^3$ GeV). This in turns translates into values of $\log_{10} f_{10}$ ranging from -52 (SUSY scale) to 0 (GUT scale). Actually, $\log_{10} f_{10} = 0$ corresponds to a situation where all the CMB signal is coming directly from strings, and it is the absolute maximum number possible according to the definition of f_{10} . As we show in the Appendix, our Bayes factors are only slightly changed when choosing other physical scales for our lower cut-off for the prior. For r there is not quite an equivalent to the symmetry breaking scales of the universe since it is a ratio of tensors to scalars rather than on an absolute scale, so we just used the same range as for f_{10} , i.e., r ranges from 1 to 10^{-52} in our logarithmic prior analysis.

Having specified the priors, we are left with the technical question of how to compute the Bayes factors. One possibility is to compute the model probabilities directly using for example nested sampling [45–47]. Here we instead employ the Savage–Dickey (SD) density ratio [40, 41], since a model with a given kind of defects is nested within the simpler model without defects at the point $f_{10} = 0$. The Bayes factor in favour of the simpler model is then just the value of the (marginalized and

normalized) posterior at $f_{10} = 0$ divided by the prior at the same point. For our linear prior in the defect amplitude, the prior is always just equal to 1. We include an Appendix in which we describe the techniques employed in order to accurately obtain the normalized posterior values and subsequent Bayes factors.

For our analysis, we ran chains with a fiducial cosmic string fractional amplitude of $f_{10}^{\text{st}} = 0.0021$ and for models that included only one kind of extra contribution (strings ‘s’, texture ‘t’ and tensor modes ‘r’), two kinds (‘st’, ‘sr’ and ‘tr’) and all three (‘str’). We then used the SD ratio to derive the Bayes factors with respect to all nested models, e.g. ‘st’ to ‘s’ and ‘t’. In this way we built a partially redundant tree of model probabilities, starting with the basic model of ‘no defects’ which we used as the reference for defining relative probabilities. The partial redundancy allowed us to check whether the results from different paths through the model space are consistent: it is for example possible to reach the ‘st’ model through the sequence ‘no defects’ \rightarrow ‘s’ \rightarrow ‘st’ as well as through ‘no defects’ \rightarrow ‘t’ \rightarrow ‘st’. The Bayes factor from both sequences must agree within the error bars. Indeed this is the case for all results quoted in the paper.

A. Analysis for linear prior

We first performed the analysis described above using linear priors for all the three extra components. Figure 5a shows the results from this exercise, in the shape of a cube with each axis denoting the presence of strings, textures and tensors respectively. The model in the lower left corner of the cube is the ‘no defect’ model while the diagonally opposite corner corresponds to ‘str’. The numbers given denote $\ln B$, with positive values for models that are favoured over the ‘no defect’ case. The fiducial string amplitude was chosen so that there is strong evidence for the presence of strings, which means that it is difficult to evaluate the SD ratio far out in the tail of the distribution in the ‘s’ case. The Appendix discusses how we evaluated SD ratios for these cases. We notice that the only other model with a positive evidence is ‘t’, which is due to the partial degeneracy of the strings and textures. The ‘r’, ‘rt’ and ‘rts’ models are significantly disfavoured.

Given these results we would conclude that there is strong evidence in favour of defects – indeed, this is about the minimal string contribution for which CMBPol would be able to make such a statement. We notice that in a parameter estimation context, the significance is 5σ if we only fit for the *correct* component (supposing we know which that component is), and it is a borderline detection when fitting for all three components (of order 3σ).

As in the parameter estimation case, we would still not be able to distinguish decisively between strings and texture, although strings are favoured by a factor of roughly 40 ($\Delta \ln B = 3.7$). To be able to pinpoint strings as the origin of the observed signal would require either a larger defect amplitude or else a more sensitive probe.

¹ In this section we will refer to the model with no extra ingredients as the ‘no defect’ model, meaning a model without strings or textures, but also without tensors.

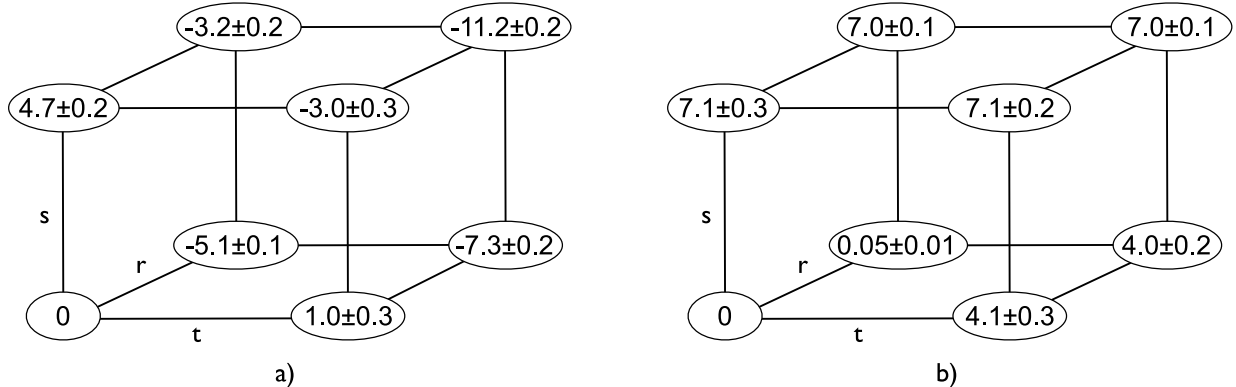


FIG. 5: Pictorial representation of the logarithm of the Bayes factors for different models, relative to a model with ‘no defect’. The lower left corner of the cube corresponds to the ‘no defect’ model, and the axes of the cube correspond to adding strings (s), textures (t) or tensors (r). Thus, the diagonally opposite corner corresponds to a model with strings+textures+tensors. Figure a) depicts a model comparison with linear priors in f_{10} , whereas in figure b) we have used a logarithmic prior instead.

B. Analysis for logarithmic prior

We also performed a model selection analysis using logarithmic priors for the extra parameters. Obtaining SD ratios for this case is even harder than for the linear case, since it presents the additional difficulty that the models are not actually nested, since $f_{10} = 0$ is not attainable (recall that the range for our priors is $\log_{10} f_{10} \in [-52, 0]$). The Appendix deals with the techniques used to obtain the SD ratios, and in this section we just present and discuss the results.

The outcome of this exercise should be very different to the one obtained with linear priors: for any prior range, the vast majority of the priors are always equivalent to the no-defect model. Therefore it is much harder to rule out defects if they are wrong as they will make the same predictions as no-defect in too much of their prior space. We can only get a signal if in some part of those prior spaces we can get a much better fit, which will enable us to rule out the no-defect case if there are defects.

We thus expect models without strings to all be indistinguishable from each other, and the models with strings to all be indistinguishable from each other. In fact, this is roughly what we see in Fig. 5b, where the results for the logarithmic prior case are shown. As it can be seen, all models containing strings are now strongly favoured ($\ln B \approx 7$). Tensors alone have a Bayes factor similar to the no-defect model. However, models with texture but no strings also get support ($\ln B \approx 4$), due to the degeneracy between strings and textures. This allows us to conclude that models with defects (strings or textures) are actually favoured with respect to the no-defect model. However, as in the linear case, it is not conclusive in distinguishing between strings and textures, even though models with strings have the highest Bayes factors.

VI. CONCLUSIONS

Simulating data as per the CMBPol mission concept study, propagating uncertainties due to foreground residuals, we find that the level of cosmic strings and textures that can be detected and correctly identified (at 3σ) by CMBPol is 0.002 and 0.001 of the total TT power spectrum at multipole 10 respectively (correspondingly, $G\mu \simeq 9 \times 10^{-8}$ for strings and $G\mu \simeq 1.4 \times 10^{-7}$ for textures). Similarly a tensor fraction of 0.0018 should be discernible. Contributions from strings and textures are highly correlated with each other, so at lower levels the signal would be harder to attribute to one or the other conclusively. Tensors are not much correlated with strings but are somewhat correlated with textures.

We also performed a model selection analysis for a fiducial model containing cosmic strings. Using a flat prior on f_{10} , we found that a model with only strings is favored over all models but the texture-only model is also better than a model without any defects. Models with several types of defects are all strongly disfavored because of a large ‘Occam’s razor’ factor. This changes when taking a prior that is flat in $\log_{10}(G\mu)$. In this case, it is not possible to rule out the presence of defects, and all models containing strings are strongly favoured (with models containing textures but no strings having an intermediate probability).

A CMBPol-like experiment, as has been proposed both in the US and Europe, has the ability to illuminate us on important issues regarding high-energy physics in the early universe, that we can only speculate about at this time. It is roughly two orders of magnitude better (in f_{10}) than what we can achieve at this point with WMAP, and over an order of magnitude better than what the Planck mission will achieve.

Appendix A: Posterior calculation for the Savage–Dickey density ratio

In this appendix we summarise the different techniques used in this work to perform the model selection analysis. In both prior choices (linear and logarithmic) for the defect contribution, we encounter challenges in obtaining an accurate normalized posterior. We will explain those challenges and describe how we overcame them.

For both prior choices, the interval for the parameter characterizing the string contribution is much wider than the precision of CMBPol, which leads to a significant “Occam’s razor” factor. For example, if the posterior was Gaussian with a variance of σ^2 and the prior flat with a width of 1, then its normalization alone contributes a factor

$$\frac{1}{\sqrt{2\pi\sigma^2}} \gtrsim 300 \quad (\text{A1})$$

in favour of the simpler no-strings model, where we used the variance of the string contribution discussed earlier. In order to strongly support the presence of strings, we need to overcome this factor as well as reach down to at least $\exp(-5) \approx 1/150$ with the posterior. We therefore need to have an accurate estimate of the posterior over four to five orders of magnitude. A normal MCMC chain would need to be exceedingly long to reach that far out; we would effectively be counting only every 50,000-th sample! This problem can be alleviated by running MC chains at higher temperatures (we used $T = 2$, and $T = 4$ where necessary) that probe the tails much better. This increases the computational cost of using the SD ratio, but not prohibitively, especially since we found that scaled versions of the $T = 1$ covariance matrix were sufficient to use for the proposal densities of the higher-temperature chains. For $T \neq 1$ we are not sampling from the desired probability density but from $\exp(-\lambda/T)$ where $\lambda = -\ln \mathcal{L}$ with \mathcal{L} is the likelihood. If we scaled the Gaussian proposal distribution the same way, then the covariance matrix C_1 at temperature T_1 should be changed to $C_2 = C_1(T_2/T_1)$. What we did in practice was to increase the proposal scale in CosmoMC from 2.4 to 3.6 whenever we doubled the temperature, i.e. an increase by a factor of 1.5 (close to the theoretical value of $\sqrt{2}$), which worked very well.

In order to use a chain with $T \neq 1$ for model selection and parameter estimation, we need to correct for the temperature. This can be done through importance sampling, by adjusting the sample weights w_i ,

$$w_i(T = 1) = w_i(T) \frac{\mathcal{L}(T = 1)}{\mathcal{L}(T)} = w_i(T) \frac{e^{-\lambda}}{e^{-\lambda/T}}. \quad (\text{A2})$$

Figure 6 shows four chains for different temperatures that use the correction given above. The resulting probability densities agree well in the high-probability peak, but the high- T chains probe the low-probability regions much better.

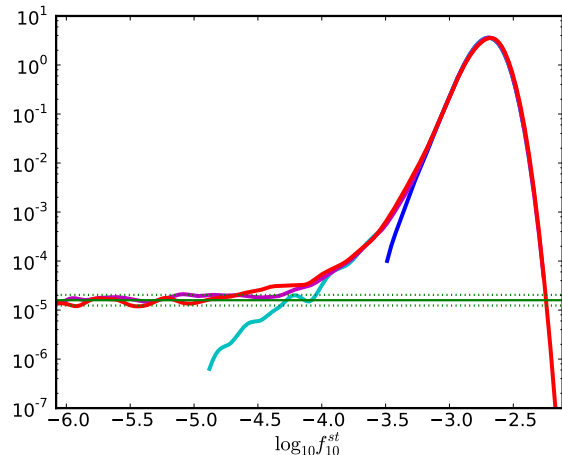


FIG. 6: The marginalized probability distribution function for f_{10}^{st} in the logarithmic prior case for four different temperatures: $T = 1$ (blue), $T = 2$ (cyan), $T = 4$ (magenta) and $T = 8$ (red) [the curves with lower temperatures end at higher f_{10}^{st}]. All chains agree in the high-probability region near $\log_{10} f_{10}^{\text{st}} = -2.7$, but only the two highest temperature chains can probe the low-probability tail which is reached for $f_{10}^{\text{st}} \rightarrow 0$.

The logarithmic prior presents the additional difficulty that the models are not actually nested since $f_{10} = 0$ is not attainable. However, we know from the previous discussion about parameter constraints that, e.g., a defect fraction of $f_{10} = 10^{-6}$ is completely undetectable by CMBPol and corresponds for all practical (although maybe not for philosophical) purposes to a model without defects. For this reason, the Bayes factor of the model with $f_{10} = 10^{-6}$ relative to the more general model with arbitrary defect contribution is the same as the one of a model with $f_{10} = 0$. But the former model *is* nested in the general model and allows us to compute the Bayes factor with the help of the SD ratio.

Additionally we do not want to sample all the way down to very big negative values of $\log_{10} f_{10}$ in the chains (in our case $\log_{10} f_{10} = -52$), since we already know that the posterior will be flat once we are below the detection threshold for the defects (see Fig. 6). For this reason we impose a cut-off for the chains at a not so tiny value of f_{10} (in the example described in the main text, we used $f_{10} = 10^{-6}$). This cut-off is arbitrary as long as it is in the asymptotic region where the posterior has become flat since defects are no longer detected. In addition, it is better to choose it slightly lower than the value at which we evaluate the SD ratio in order to avoid edge effects.

We proceed as follows: first we evaluate the posterior at the chosen point (in our example, $\log_{10} f_{10} = -6$). Note that the value obtained is normalized to the width of the prior actually used in the calculation (in \log_{10} units, the width is $\epsilon = 6$). Since we are in the region where the posterior is already flat, we add a stretch of width Δ (in our example $\Delta = 46$ to reach $\log_{10} f_{10} = -52$), but we

have to be careful with normalization, since the posterior has now to be normalized taking into account this new stretch. Let us denote by q the value measured at the cut-off point inside the asymptotic region (e.g. $q = 1.6 \times 10^{-5}$ in Fig. 6). Then, the normalized posterior actually has a value of $p = q/(1 + q\Delta)$. The prior is flat over the whole range so that its value is $1/(\Delta + \epsilon)$ and hence the Bayes factor is

$$B = \frac{1 + q\Delta}{q(\Delta + \epsilon)}. \quad (\text{A3})$$

It is worth checking how much the Bayes factor changes for different values Δ . Recall that Δ basically gives us the lower energy scale taken into account in the prior for $\log_{10} f_{10}$. For example, $\Delta = 46$ corresponds to SUSY breaking scale, and $\Delta = 50$ would correspond to the electroweak scale. It is easy to verify that $\ln B(\Delta = 46) \sim 7.09$ and $\ln B(\Delta = 50) \sim 7.01$, so a wide range of lower cutoffs would give virtually the same results.

Unfortunately there is one additional hurdle that needs to be overcome. In the model analysis we have performed, we often need to fit for several kinds of components: strings (s), textures (t) and tensors (r); and combinations of them: ‘st’, ‘sr’, ‘tr’ and ‘str’ models. In order to compute SD ratios for models with more than one component, we marginalize over all but one component. However, this marginalization should be done not over the limited range of f that we actually sample from, but over the full range (taking account the stretch Δ in all extra components).

We illustrate how this was performed in the concrete example ‘st’ \rightarrow ‘s’, where the simulated range of the parameters is smaller than the full range both in f_{10}^{st} and in f_{10}^{tex} . First we get the weight of the full simulated chain $W_{\text{st}}^{\text{sim}}$, and the (normalized) pdf $p_{\text{st}}^{\text{sim}}$ of the ‘st’ chain by marginalizing over all parameters except f_{10}^{tex} . That would be enough if our model was nicely nested and we did not have to add the stretch Δ . To account for the stretch, we consider the interval of unit width

$\log_{10} f_{10}^{\text{st}} \in [-6, -5]$ of the ‘st’ chain. We calculate both its weight $W_{\text{st}}^{(1)}$ and its normalized pdf $p_{\text{st}}^{(1)}$, once again by marginalizing over all parameters except f_{10}^{tex} . Note that $p_{\text{st}}^{(1)}$ should be the same as the pdf obtained from the ‘t’ chains, since $p_{\text{st}}^{(1)}$ is calculated virtually in the region with only textures (no strings). We verified that this was the case.

We now have all the ingredients that are necessary to marginalize over the full range: Let $W_{\text{st}}^{\Delta} = \Delta \times W_{\text{st}}^{(1)}$ be the estimated weight over all the Δ stretch. Then the normalized marginalized pdf for the full range is given by

$$p_{\text{st}}^{\text{full}} = \frac{p_{\text{st}}^{(1)} W_{\text{st}}^{\Delta} + p_{\text{st}}^{\text{sim}} W_{\text{st}}^{\text{sim}}}{W_{\text{st}}^{\Delta} + W_{\text{st}}^{\text{sim}}} \quad (\text{A4})$$

We still have to account for the Δ stretch in f_{10}^{tex} , but we are just in the case tackled earlier in this section, and one just needs to apply Eq. (A3) to get the Bayes factor.

Acknowledgments

We are grateful for useful discussions with José Juan Blanco-Pillado, Julian Borrill, Anthony Challinor, Marina Cortes, Stacey-Jo Dias, Juan García-Bellido and Antony Lewis. We acknowledge support from the Science and Technology Facilities Council [grant number ST/F002858/1] and the Swiss NSF (M.K.). J.U. and M.K. thank the Benasque Centre for Science, where part of this work was done, for hospitality. This work was partially supported by the Basque Government (IT-559-10), the Spanish Ministry FPA2009-10612, and the the Spanish Consolider-Ingenio 2010 Programme CPAN (CSD2007-00042) (J.U.). The analysis was performed on the Archimedes cluster of the University of Sussex and the Andromeda cluster of the University of Geneva.

-
- [1] G. Hinshaw et al. (WMAP), *Astrophys. J. Suppl.* **180**, 225 (2009), 0803.0732.
 - [2] M. R. Nolte et al. (WMAP), *Astrophys. J. Suppl.* **180**, 296 (2009), 0803.0593.
 - [3] J. Dunkley et al. (WMAP), *Astrophys. J. Suppl.* **180**, 306 (2009), 0803.0586.
 - [4] N. Jarosik et al. (2010), 1001.4744.
 - [5] D. Larson et al. (2010), 1001.4635.
 - [6] E. Komatsu et al. (WMAP), *Astrophys. J. Suppl.* **180**, 330 (2009), 0803.0547.
 - [7] E. Komatsu et al. (2010), 1001.4538.
 - [8] M. Wyman, L. Pogosian, and I. Wasserman, *Phys. Rev. D* **72**, 023513 (2005), astro-ph/0503364.
 - [9] A. A. Fraisse, *JCAP* **0703**, 008 (2007), astro-ph/0603589.
 - [10] R. A. Battye, B. Garbrecht, and A. Moss, *JCAP* **0609**, 007 (2006), astro-ph/0607339.
 - [11] N. Bevis, M. Hindmarsh, M. Kunz, and J. Urrestilla, *Phys. Rev. Lett.* **100**, 021301 (2008), astro-ph/0702223.
 - [12] L. McAllister, E. Silverstein, and A. Westphal, *Phys. Rev. D* **82**, 046003 (2010), 0808.0706.
 - [13] R. Kallosh and A. D. Linde, *JCAP* **0704**, 017 (2007), 0704.0647.
 - [14] M. Majumdar and A. Christine-Davis, *JHEP* **03**, 056 (2002), hep-th/0202148.
 - [15] S. Sarangi and S. H. H. Tye, *Phys. Lett. B* **536**, 185 (2002), hep-th/0204074.
 - [16] N. T. Jones, H. Stoica, and S. H. H. Tye, *Phys. Lett. B* **563**, 6 (2003), hep-th/0303269.
 - [17] R. Jeannerot, J. Rocher, and M. Sakellariadou, *Phys. Rev. D* **68**, 103514 (2003), hep-ph/0308134.
 - [18] A. Vilenkin and E. P. S. Shellard, *Cosmic Strings and*

- Other Topological Defects* (Cambridge University Press, Cambridge, U.K., 1994).
- [19] M. B. Hindmarsh and T. W. B. Kibble, Rept. Prog. Phys. **58**, 477 (1995), hep-ph/9411342.
 - [20] D. H. Lyth and A. Riotto, Phys. Rept. **314**, 1 (1999), hep-ph/9807278.
 - [21] U. Seljak and A. Slosar, Phys. Rev. **D74**, 063523 (2006), astro-ph/0604143.
 - [22] L. Pogosian and M. Wyman, Phys. Rev. **D77**, 083509 (2008), arXiv:0711.0747 [astro-ph].
 - [23] N. Bevis, M. Hindmarsh, M. Kunz, and J. Urrestilla, Phys. Rev. **D76**, 043005 (2007), arXiv:0704.3800 [astro-ph].
 - [24] J. Urrestilla, P. Mukherjee, A. R. Liddle, N. Bevis, M. Hindmarsh, and M. Kunz, Phys. Rev. **D77**, 123005 (2008), 0803.2059.
 - [25] Planck satellite, ESA, URL <http://www.rssd.esa.int/index.php?project=Planck>.
 - [26] D. Baumann et al. (CMBPol Study Team), AIP Conf. Proc. **1141**, 10 (2009), 0811.3919.
 - [27] U.-L. Pen, U. Seljak, and N. Turok, Phys. Rev. Lett. **79**, 1611 (1997), astro-ph/9704165.
 - [28] R. Durrer, M. Kunz, and A. Melchiorri, Phys. Rept. **364**, 1 (2002), astro-ph/0110348.
 - [29] N. Bevis, M. Hindmarsh, and M. Kunz, Phys. Rev. **D70**, 043508 (2004), astro-ph/0403029.
 - [30] J. Urrestilla, N. Bevis, M. Hindmarsh, M. Kunz, and A. R. Liddle, JCAP **0807**, 010 (2008), arXiv:0711.1842 [astro-ph].
 - [31] M. Cruz, N. Turok, P. Vielva, E. Martinez-Gonzalez, and M. Hobson, Science **318**, 1612 (2007), 0710.5737.
 - [32] N. Bevis, M. Hindmarsh, M. Kunz, and J. Urrestilla, Phys. Rev. **D75**, 065015 (2007), astro-ph/0605018.
 - [33] A. Achúcarro and T. Vachaspati, Phys. Rept. **327**, 347 (2000), hep-ph/9904229.
 - [34] A. Achúcarro, P. Salmi, and J. Urrestilla, Phys. Rev. **D75**, 121703 (2007), astro-ph/0512487.
 - [35] R. Battye, B. Garbrecht, and A. Moss, Phys. Rev. **D81**, 123512 (2010), 1001.0769.
 - [36] N. Bevis, M. Hindmarsh, M. Kunz, and J. Urrestilla, Phys. Rev. **D82**, 065004 (2010), 1005.2663.
 - [37] L. Verde, H. Peiris, and R. Jimenez, JCAP **0601**, 019 (2006), astro-ph/0506036.
 - [38] A. Lewis, Phys. Rev. **D71**, 083008 (2005), astro-ph/0502469.
 - [39] A. Lewis and S. Bridle, Phys. Rev. **D66**, 103511 (2002), astro-ph/0205436.
 - [40] I. Verdinelli and L. Wasserman, J. Am. Statist. Assoc. **90**, 614 (1995).
 - [41] R. Trotta, Mon. Not. Roy. Astron. Soc. **378**, 72 (2007), astro-ph/0504022.
 - [42] J. Garcia-Bellido, R. Durrer, E. Fenu, D. G. Figueroa, and M. Kunz (2010), 1003.0299.
 - [43] L. Pogosian and T. Vachaspati, Phys. Rev. **D60**, 083504 (1999), astro-ph/9903361.
 - [44] R. Battye and A. Moss, Phys. Rev. **D82**, 023521 (2010), 1005.0479.
 - [45] J. Skilling, AIP Conference Proceedings **735**, 395 (2004), URL <http://link.aip.org/link/?APC/735/395/1>.
 - [46] P. Mukherjee, D. Parkinson, and A. R. Liddle, Astrophys.J. **638**, L51 (2006), astro-ph/0508461.
 - [47] B. A. Bassett, P. S. Corasaniti, and M. Kunz, Astrophys.J. **617**, L1 (2004), astro-ph/0407364.